Journal of Electromagnetic Waves and Applications

ISSN: (Print) (Online) Journal homepage: https://www.tandfonline.com/loi/tewa20

NLFM pulse radar for drone detection using predistortion technique

Ashish Kumar Singh , Kyung-Bin Bae & Seong-Ook Park

JOURNAL OF ELECTROMAGNETIC WAVES AND APPLICATIONS
2021, VOL. 35, NO. 3, 416–429
https://doi.org/10.1080/09205071.2020.1844598

NLFM pulse radar for drone detection using predistortion technique

Ashish Kumar Singh [a], Kyung-Bin Bae [b] and Seong-Ook Park [b]

[a]Information & Electronics Research Institute, KAIST, Daejeon, Republic of Korea; [b]School of Electrical Engineering, KAIST, Daejeon, Republic of Korea

ABSTRACT

The development of radar technology for the detection of small drones is getting attention of researchers. In this work, the detection of drones using Ku-band radar system has been discussed. We have utilized the advantage of nonlinear frequency modulation (NLFM) waveform for the suppression of range sidelobes. The performance and sensitivity of a radar system can be related with the linearity of system response. Here, we have made an effort to minimize non-linearity in the radar system response by using digital predistortion method. In this method, amplitude weighting coefficients have been calculated based on the received data. We have used FPGA-based transceiver for intermediate frequency (IF) signal generation and data acquisition, along with Ku-band up-down converters. The radar system was first calibrated for desired frequency band using amplitude predistortion method. In this article, experiment results for the detection of single drone and two drones using NLFM pulse signal are presented.

ARTICLE HISTORY
Received 25 June 2020
Accepted 24 October 2020

KEYWORDS
Drones; non-linear frequency modulation; predistortion; pulse compression; radar detection

1. Introduction

In last decade, the application of unmanned aerial vehicles (UAVs) especially smaller drones has been drastically increased due to the advancement of manufacturing technologies. Newer drones are now capable of flying higher with faster speed to longer range and for longer time with/without payloads [1,2]. UAVs may be equipped with different types of sensors such as IR and video camera. These UAVs are advantageous for various applications including defense, surveillance, safety inspection and medical field (for delivering purpose) [3]. However, drones are now major concerns about privacy and safety. It is also possible to transport dangerous and/or restricted materials using drones [4,5]. Some efforts are made in the field of drone detection and classification using radar systems [6,7]. In previous work, the development of distributed frequency-modulated continuous-wave (FMCW) radar system for drone detection has been described in [8]. The extraction of micro-Doppler signature using radar system is crucial for classification purpose. Micro-Doppler parameter extraction has been studied in [9,10].

CONTACT Ashish Kumar Singh ashish@kaist.ac.kr Information & Electronics Research Institute, KAIST, Daejeon, Republic of Korea

The requirement of the radar system with the sidelobe suppression is essential for reducing the interference between two targets, and hence improving the overall performance in the detection and estimation of target range [11]. Range sidelobes of a target with large RCS can affect the detection of the smaller target and also results in range ambiguity. Amplitude tapering of the transmitted waveform is one of the candidates for sidelodes suppression. The effectiveness of amplitude tapering on pulse compression is correlated with the linearity of a radar system response. However, most of the radar system exhibits some nonlineraties in due to power amplifier [12]. Pulse compression technique utilizing Non-Linear Frequency Modulation (NLFM) signal can exhibit lower sidelobes as compared to Linear Frequency Modulation (LFM) signal [13,14]. Applications of NLFM waveform for precipitation radar and space-borne cloud radar systems were presented in [15].

Modern radar systems utilize various signals for better detection and tracking of the target. The performance of pulse compression radar system mostly depends on the quality of actual transmitted and received signals [16,17]. The phase-coded waveform has discontinuous phase and amplitude weighted waveform shows amplitude variability, these can cause increase in mismatch loss at the receiver (Rx) end. LFM waveform has constant amplitude and continuous phase [14]. Whereas the matched filter response of LFM has higher sidelobes level. In order to improve the peak to sidelobe ratio (PSLR), several optimization methods such as windowing technique and adaptive filtering can be used, but these techniques reduce the SNR level. In contrast, the matched filter output of NFLM waveform exhibits lower level side-lobes without loss of the SNR. Signals such as NLFM chirp signals and polyphased coded waveform are sensitive to the linearity of radar components. The linearity performance of nearly all amplifiers change with respect to frequency. Nonlinearity in any radar system is mostly caused by High Power Amplifier (HPA) and Low Noise Amplifier (LNA) [18]. Therefore, the performance of matched filter deviates from the desired behavior. The requirement of linearization techniques for radar system is very essential [19–21]. One of the methods is to implement a predistorter block such that it cancels or minimizes the non-linearity distortion of the system [22,23]. Predistortion techniques may be realized as analog predistortion [24] or digital predistortion [25].

The work presented in this article focuses on the effectiveness of NLFM chirp signal with amplitude predistortion technique for the detection of drones using pulse radar system. To the extent of our knowledge, this is the first work that study the NLFM-based pulse radar system for drone detection. We also believe that there was no previous research that focuses on the extraction of micro-Doppler signature using NFLM pulse signal. First, NLFM signal has been used because of it lower sidelobes level as compared to LFM signal. Simulation result confirms the theory and NLFM waveform with desired specification was used for pulse radar system. We have utilized Field Programmable Gate Array (FPGA)-based transceiver for intermediate frequency (IF) signal generation and data acquisition, along with Ku-band up/down converter. Second, we have analyzed the radar system for the identification of nonlinearty, using various loopbacks. Nonlinearity in the radar system was mainly caused by transceiver, HPA and LNA blocks. We have utilized the digital predistortion technique because it is cost effective, reliable and power efficient [22]. Finally, experiments have been carried out for drone detection using the linearized radar system.

The rest of this article is structured as follows. In Section 2, basic concept of NLFM signal is presented along with simulation result. Amplitude predistortion technique for linearization of radar system is given in Section 3. Drone detection experiments have been performed using commercially available drones, and result analysis is presented in Section 4. Finally, some important conclusions are drawn in Section 5.

2. NLFM chirp signal

Chirp signal is a sinusoidal signal whose frequency sweeps through an entire range of frequency band, within a specific time period. It is mostly applied to radar systems for improving range resolution and Doppler resolution. If the frequency of a chirp signal increases with time, it is known as Up-chirp. However, if the frequency decreases, it is referred as Down-chirp. A chirp signal can be either up-chirp, down-chirp or combination of both. Based on the frequency functions, chirp signals can be categorized into two types, i.e. linear frequency modulation (LFM) and nonlinear frequency modulation (NLFM) signal [26,27]. The instantaneous frequency of an LFM signal changes linearly with time. A general expression of LFM signal is given as

$$s(t) = a(t) \cdot e^{j2\pi\phi(t)} \tag{1}$$

$$\phi(t) = \alpha_0 \cdot t + \alpha_1 \frac{t^2}{2}, \quad 0 \le t < T \tag{2}$$

where α_0 and α_1 are the starting frequency and the chirp rate, respectively. Here, $a(t)$ and $\phi(t)$ denote the time-varying amplitude and time-varying phase functions.

LFM-based radar system utilizes pulse compression technique in order to improve its overall performance such as detection capability, signal to noise ratio (SNR) and range resolution. Pulse compression is accomplished by correlating the transmitted waveform with the radar received signal. Pulse compression ratio is defined as a ratio of the transmitted pulse duration to the compressed pulse duration. It also represents the time-bandwidth product of the radar system. Windowing is basically an amplitude weighting of transmitted waveform and it has been used for range-sidelobe suppression of pulse compression [28,29].

A chirp signal with its frequency sweeping as a non-linear function of time is called as NLFM signal. NLFM signal inherently suppresses sidelobe level, without opting the amplitude weighting function. Thus it preserves the maximum SNR performance of the system. However, pulse compression of NLFM signal also results in broadening of mainlobe [29]. The frequency sweep function of NLFM waveform is represented as

$$f(t) = f_0 + k \cdot t + \frac{\beta}{\pi} B \cdot \sin(2\pi \cdot B \cdot t) \tag{3}$$

where f_0, B and β are center frequency, bandwidth and a design parameter, respectively. For $\beta = 0$, the equation converse to LFM waveform.

We have generated LFM and NLFM waveforms using MATLAB. Detailed specifications of chirp waveforms are given in Table 1. The frequency range is from $-B/2$ to $B/2$, where B is total bandwidth of chirp signals. The design parameter β for NFLM waveform is 0.2.

The comparisons of frequency function and auto-correlation for LFM and NFLM signals are given in Figure 1. We have shown zoomed result for autocorrelation function for easy comparison of the sidelobes. It is clear from the autocorrelation result that NFLM waveform has lower sidelobe level as compared to the LFM waveform. Thus we have considered

Table 1. Signal specifications.

Parameter	Value
Center frequency (f_0)	0 Hz
Bandwidth (B)	30 MHz
Number of samples (N)	1000
Sweep time (T)	16.276 μs
Sampling frequency (F_s)	61.44 MHz

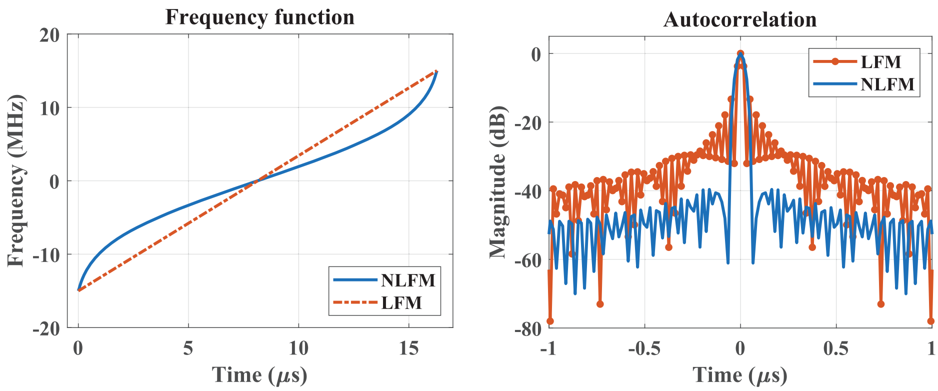

Figure 1. Simulation results of NLFM and LFM waveform: (a) frequency as a function of time and (b) autocorrelational results for LFM and NLFM waveforms.

NLFM signal with same specification for further experiment using Ku-band up/down converters. In the following section, predistortion technique is briefly described and amplitude predistortion for linearization of the radar system has been explained.

3. Predistortion technique

The basic idea of digital predistortion (DPD) is to introduce a component to existing radar system which has inverse distortion characteristics. Hence, it will cancel out the non-linear distortion due to RF amplifiers and a linear response of the radar system can be achieved. DPD can be realized by distorting the original input signal such that when the signal is subjected to a system, the desired output signal is achieved as a resultant of distortions caused by system response [22]. Thus it is feasible to compensate the nonlinearity in the system response.

Digital predistortion utilized for compensating the non-linearity effect prior to the power amplifier, and possible to operate the radar system nearer to the maximum rated power as well preserving low spectral regrowth [23,25]. Predistortion method may be performed in either time domain and/or frequency domain.

In this work, we are utilizing NLFM waveform for pulse radar system. Because the power spectrum of NLFM signal is not flat throughout the frequency range, we have considered time-domain based amplitude predistortion technique. One of the DPD methods is amplitude predistortion, which involves the estimation of the amplitude weighting function based on the envelope of distorted signal [30]. The estimation of envelopes is one of the

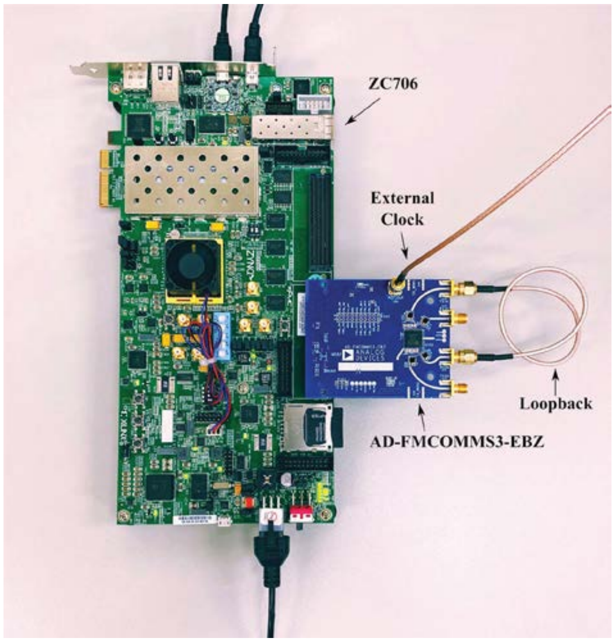

Figure 2. Photograph of FPGA-based transceiver.

essential steps. In order to achieve desired output, fine tuning and modification was applied while the estimation of lower and upper envelopes. The inverse of estimated envelope is used as coefficient and it acts as amplitude weight for original signal. Additional smoothing filter was implemented for further tuning of the estimated envelope. Moreover, iterating the overall process may be necessary, if there is some deviation in the system response. The amplitude predistorted waveform ($x_{ap}(n)$) was obtained by multiplying the coefficient ($w_{coef}(n)$) with the original waveform ($x(n)$).

$$x_{ap}(n) = w_{coef}(n) \cdot x(n) \tag{4}$$

3.1. FPGA-based signal generation

We are using Xilinx's ZC706 FPGA evaluation board along with Analog Devices' AD-FMCOMMS3-EBZ transceiver board for NLFM signal generation and data acquisition. One of the ways to generate desired chirp signal is by loading the original signal data to DAC buffer memory of FPGA. The waveform data files can be created by MATLAB or C program.

The FPGA-based transceiver setup for loop-back test is shown in Figure 2. The transceiver has two transmitters and two receivers on board. The sampling frequency of the DAC and ADC is 61.44 MSPS. Xilinx Vivado has been used for HDL project implementation and programming the FPGA. Linux is running on ARM softprocessor of ZC706 board. The program uses libiio Linux kernel for communication and control of transceiver. MATLAB/Simulink model or IIO oscilloscope may be used for signal generation and signal acquisition.

Radar system was implemented using FPGA-based transceivers for IF signal generation and receiving the data. We have used MATLAB for generating 0 ± 15 MHz NLFM waveform

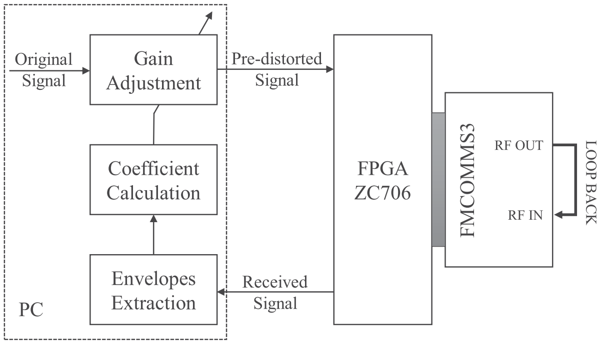

Figure 3. Block diagram of digital pre-distortion (DPD) technique.

and load the waveform in the FPGA for transmitting the signal at a center frequency of 140 MHz with 30 MHz bandwidth. We have analyzed both channels in loopback and identified the nonlinearlity in transceiver. We have to compensate this nonlinearity by using pre-distortion technique. We have used digital pre-distortion (DPD) as shown in Figure 3.

In this technique, the waveform is passed through a predistorter to modify the amplitude such that output of ADC will be linear. Finally, we have used amplitude weighting function to compensate loss at higher frequency. Figure 4 shows the digital pre-distortion processing steps for the loopback. Here, the envelope of received signal has been estimated. The upper and lower envelopes were extracted from the distorted signal using a sliding window. The coefficient values based on upper and lower envelopes have been calculated for each sample points. The predistorted signal was determined by multiplying the coefficient values with the original signal.

Resulting predistorted waveform is once again sent through the loopback system. The comparison of acquired waveform before and after employing the predistortion technique is shown in Figure 5.

3.2. Linearization of radar system

We have used super-heterodyne radar system operating at a center frequency of 14.1 GHz. Here, FPGA-based transceiver system was combined with the Ku-band up-converter and down-converter system as illustrated in Figure 6. For both up-converter and down-converter, two stage mixers were utilized. This approach provides a good isolation between RF and LO ports. Center frequencies of each stages are shown in Figure 6. We have considered six test points, i.e. “A” to “F” for validating the operation of subsystem in linear region.

The predistortion technique was implemented for the linearization of the radar system for five loopbacks (#1 to #5). The loopbacks are denoted by broken lines, as shown in Figure 6. Here, loop #1 is IF loopback, which has been discussed in previous section. Loopback #2 is the output of up-converter directly connected with down-converter, loopback #3 consists of up-converter followed by HPA and attenuator before feeding to down-converter, loopback #4 consists of up-converter and LNA with attenuator and loop #5 is Ku-band loopback which includes HPA and LNA. Variable attenuator was introduced to adjust the input power

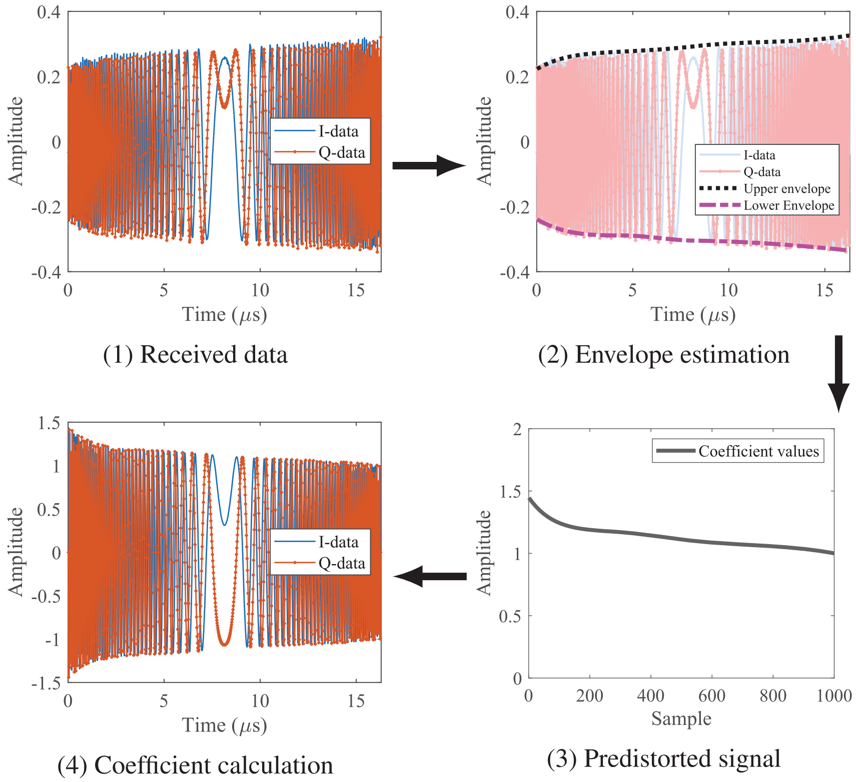

Figure 4. Processing steps of amplitude pre-distortion technique.

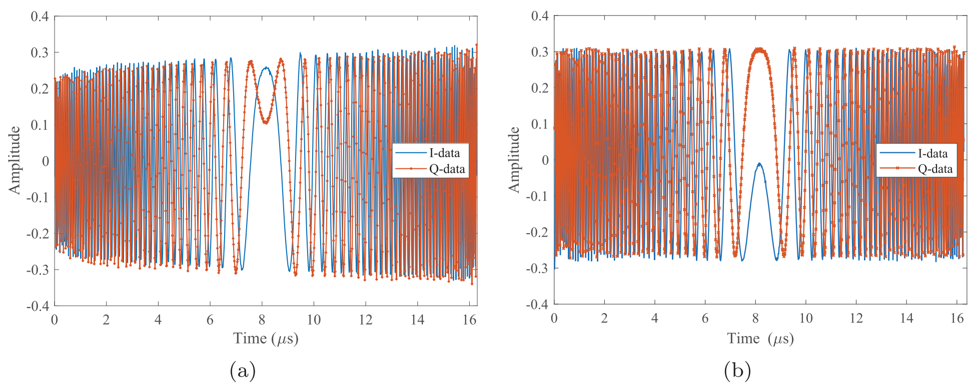

Figure 5. Comparison of received NLFM waveform after loopback (a) without predistortion and (b) with predistortion technique.

level of each subsystem, which insures that radar system operating in the linear region. A clock generator has been utilized for the synchronization of IF and RF subsystems, driven by a 200 MHz external clock oscillator. It generates 40 MHz clock for IF transceiver and two 5 MHz clocks for both up-converter and down-converter blocks.

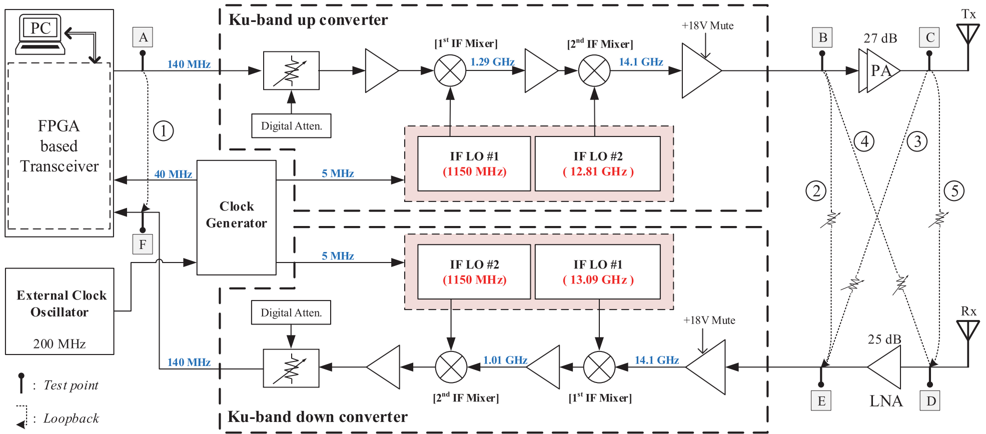

Figure 6. Block diagram of chirp pulse radar system.

(a) (b)

Figure 7. Outdoor measurement using Ku-band radar system. (a) Experiment setup, (b) photographs of commercially available quadcopters: DJI Inspire-1 (left) and DJI Inspire-2 (right).

4. Outdoor experiment

For outdoor experiment, we have attached Tx and Rx horn antennas at points "C" and "D", respectively. The measurement took place at rooftop of the our research building. Tx and Rx antennas were separated by distance of about 1.1 m, and they were pointing vertically upward. We have used Tx #1 with Rx #2 of FMCOMMS3-EBZ board, to minimize the internal leakage. Whereas second pair, consists of Tx #2 and Rx #1, was utilized for pulse signal lookback. This pulse signal acts as marker for each chirp burst. Received data consists of 500 chirp bursts. The NLFM signal was generated with 50% duty cycle, and PRI of 32.552 μs.

Figure 7(a) shows the photograph of outdoor experiment setup. Two commercially available drones, i.e. DJI Inspire-1 and DJI Inspire-2 were used as targets, as shown in Figure 7(b). Inspire 2 used as a single target and it was hovering vertically above at height varying from 20 m to 400 m. For two targets experiment, the height of DJI Inspire-2 was fixed at 100 m, whilst height of Inspire 1 was varying from 20 m to 80 m.

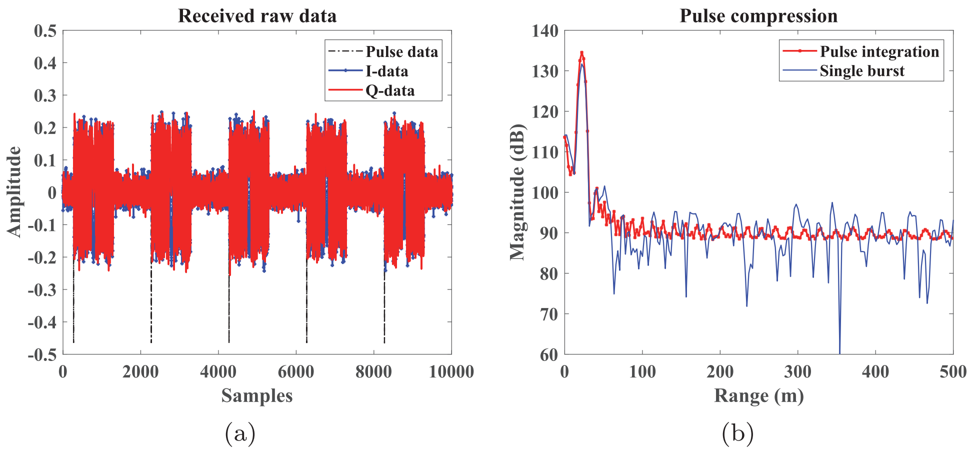

Figure 8. Radar received signal for a drone at height of 20 m: (a) raw data (I–Q data) along with pulse signal and (b) pulse compression results.

4.1. Measurement results

The acquired data from both channels were used for target detection. Here, we have used original NFLM waveform (without predistortion) for pulse compression. Each burst can be distinguished by the help of pulse signal waveform (loopback). Acquired data for both reflected signal from the target and pulse loopback signal are shown in Figure 8(a). The pulse compression result of single burst and its comparison with pulse integration of 500 bursts are shown in Figure 8(b).

Here, the range resolution of the NLFM chirp waveform with a bandwidth of 30 MHz is 5 m. The sampling rate of data acquisition may also limit the accuracy of range measurement. When the received data is sampled at low frequency, say near to Nyquist frequency. The desired (ideal) peak of range compression result may occur in between two sample points. Deviation in range (δR_d) due to data sampling rate can be given by the following equation:

$$\delta R_d = \frac{c}{4 \cdot f_s} \tag{5}$$

where c is the speed of light and f_s is the sampling frequency. In this setup, the sampling frequency f_s of ADC is 61.44 MHz. Using Equation (4), the estimated range accuracy due to sampling rate is 1.22 m.

It is noticeable from Figure 9 that the desired peak may occur between point “A” and point “B”. Difference between two range points is 2.44 m. Thus the maximum deviation in range measurement due to data sampling is half of the difference in consecutive range points (i.e. 1.22 m). Broken line (see Figure 9) represented as an interpolated pulse compression and, it is overlapped with the calculated pulse compression of measured data. The sample points on either side of a desired peak may associate to the measured range point. And the deviation in the estimation of range peak can also cause error in the calculated peak power.

Since the antennas were placed closely, there was direct leakage between Tx and Rx. The peak at 0 m corresponds to this direct leakage signal. Therefore, it was utilized for adjusting

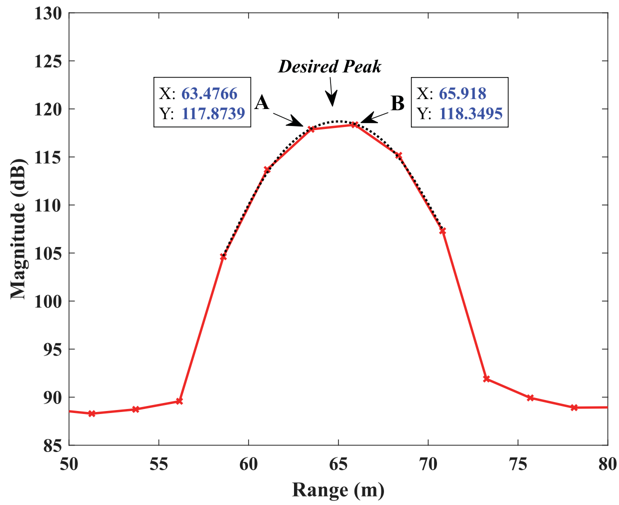

Figure 9. Comparison between pulse compression peak and desired peak.

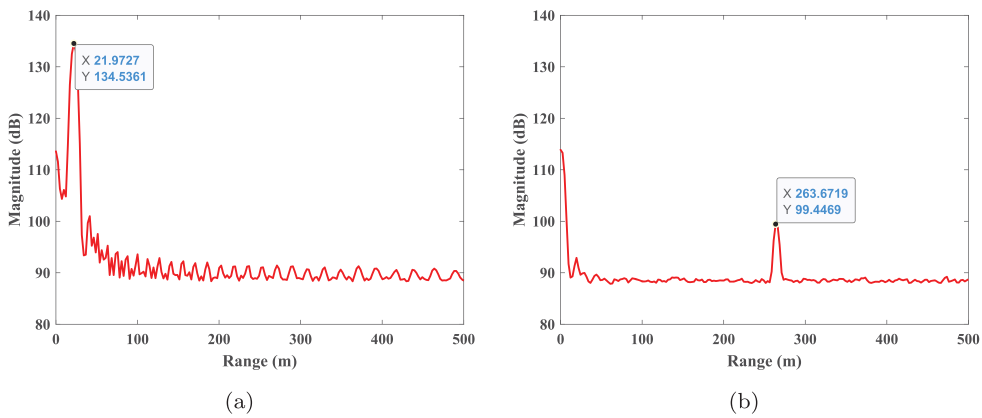

Figure 10. Pulse compression results using pulse integration for drone (Inspire-2) hovering at various heights.

range bins of pulse compression results. We have noticed that Inspire-1 has some difficulties in hovering at a fixed point, due to high wind. Thus we have considered Inspire-2 as a target for single drone experiments. We have gathered data for a total of 11 different heights (varying from 20 m to 450 m) for single drone experiment. Figure 10 presents some of the pulse integration results for single drone. Wind induces some movement of hovering drones, which results fluctuation in the measured data. Measurement results of two drones are shown in Figure 11. From the results, it is clear that the drones can be easily detectable up to 400 m.

We have compared the measured pulse compression result with the standard radar equation for single drone detection, as shown in Figure 12. It is clear that the measured result follows the power-range curve and which is inversely proportional to the fourth power of the range (i.e. $1/R^4$). Results shows that the variation in the peak power of

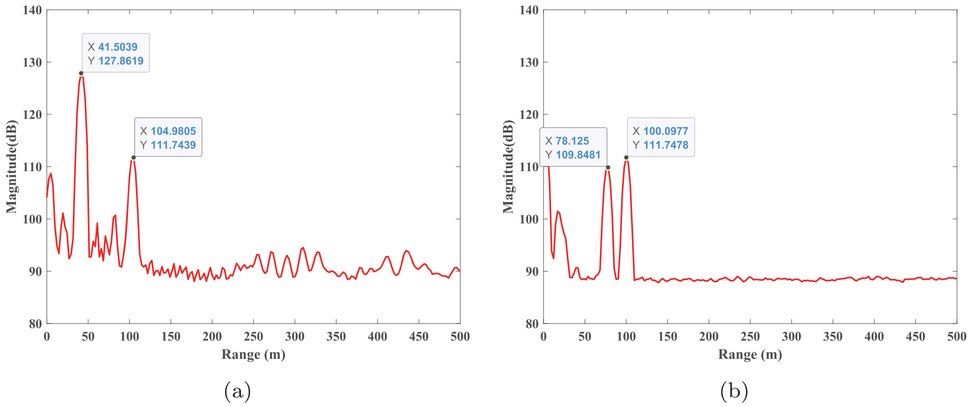

Figure 11. Pulse compression results (after pulse integration) for measurement of two drones. Inspire-2 hovering at fixed height of 100 m while height of Inspire-1 varying as (a) 40 m and (b) 80 m.

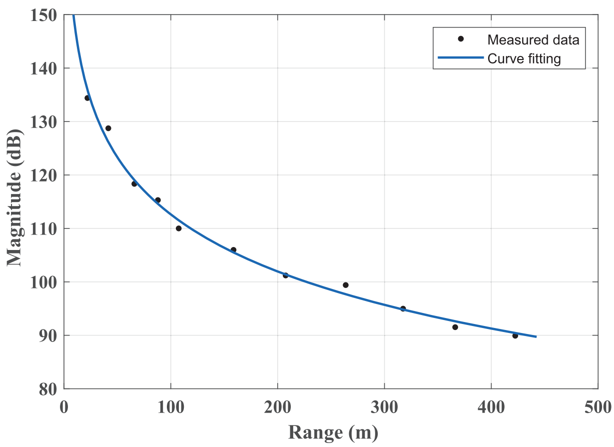

Figure 12. Comparison between drone measurement result and curve fitting result using standard radar equation.

drone with change in the range. The noise floor of pulse integration result is 88.4 dB, approximately. Noise floor is almost fixed for all the cases.

Range-velocity map using the received signal has been presented, along with micro-Doppler signature due to rotating blades of the flying drone. Pulse compression results of each burst were used for the extraction of micro-Doppler signature. It was achieved by calculating Short-time Fourier transform (STFT) along slow time.

As a typical example, range-velocity map and micro-Doppler signature for a drone flying at a height of 80 m is presented in Figure 13. Since, the drone was hovering vertically above the radar, the Doppler bandwidth caused by rotating blades is small. Measured Doppler bandwidth was 6 KHz, approximately. Hence, the micro-Doppler signature of a drone can be extracted using NLFM signal for pulse radar system. Results support the efficacy of NLFM-based radar system using DPD for the practical application of drone detection.

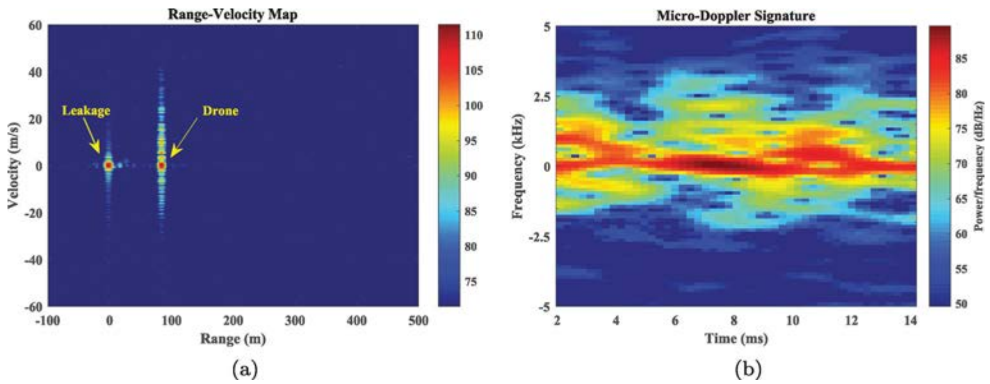

Figure 13. A typical results of (a) range-velocity map and (b) micro-Doppler signature for drone at a height of 80 m.

5. Conclusion

In this article, a pulse compression radar system using NLFM waveform was introduced for the detection of drones. The effect of NLFM waveform on sidelobe reduction was validated by simulation results. There was obvious difference between the range sidelobes of LFM and NFLM waveforms. Prior to the outdoor experiment, nonlinearity in the radar system being identified and suppressed. Here, various loopback tests have been performed and the received data was analyzed. Main cause of nonlinearity in the system response is due to IF transceiver, HPA and LNA. For the linearization of radar system response, amplitude predistortion technique has been implemented. Our Ku-band radar system exploited advantages of NLFM waveform along with predistortion technique. Outdoor experiments were performed using predistorted NFLM pulse signal. The pulse compression results with pulse integration have been presented. The measurement results were presented for single and dual targets, which support the drone detection capability of our radar system. Also, we have successfully extracted micro-Doppler signature of a drone using NFLM pulse radar system.

Disclosure statement

No potential conflict of interest was reported by the author(s).

Funding

This work was supported by the National Research Foundation of Korea (NRF) grant funded by the Korea government (MSIT) (No. 2019R1A2B5B01069407), and Institute of Information & Communications Technology Promotion & Evaluation (IITP) grant funded by the Korea government (MSIT) (No. 2018-0-01658, Key Technologies Development for Next Generation Satellites).

ORCID

Ashish Kumar Singh http://orcid.org/0000-0003-2728-6953
Seong-Ook Park http://orcid.org/0000-0002-2850-8063

References

[1] Anwar MZ, Kaleem Z, Jamalipour A. Machine learning inspired sound-based amateur drone detection for public safety applications. IEEE Trans Vehicular Technol. 2019;68(3):2526–2534.
[2] Lu M, Bagheri M, James AP, et al. Wireless charging techniques for uavs: a review, reconceptualization, and extension. IEEE Access. 2018;6:29865–29884.
[3] Rosser JC, Vignesh V, Terwilliger BA, et al. Surgical and medical applications of drones: a comprehensive review. JSLS: J Soc Laparoendoscopic Surgeons. 2018;22(3):e2018.00018. DOI:10.4293/jsls.2018.00018
[4] Luppicini R, So A. A technoethical review of commercial drone use in the context of governance, ethics, and privacy. Technol Soc. 2016 Aug;46:109–119. DOI:10.1016/j.techsoc.2016.03.003
[5] Allouch A, Koubâa A, Khalgui M, et al. Qualitative and quantitative risk analysis and safety assessment of unmanned aerial vehicles missions over the internet. IEEE Access. 2019;7:53392–53410.
[6] Patel JS, Fioranelli F, Anderson D. Review of radar classification and rcs characterisation techniques for small uavs or drones. IET Radar Sonar Navigation. 2018;12(9):911–919.
[7] Suh J, Minz L, Jung D, et al. Drone-based external calibration of a fully synchronized ku-band heterodyne fmcw radar. IEEE Trans Instrum Meas. 2017;66(8):2189–2197.
[8] Shin D, Jung D, Kim D, et al. A distributed fmcw radar system based on fiber-optic links for small drone detection. IEEE Trans Instrum Meas. 2017;66(2):340–347.
[9] Zhao Y, Su Y. Cyclostationary phase analysis on micro-doppler parameters for radar-based small uavs detection. IEEE Trans Instrum Meas. 2018;67(9):2048–2057.
[10] Zhao Y, Su Y. The extraction of micro-Doppler signal with emd algorithm for radar-based small uavs' detection. IEEE Trans Instrum Meas. 2020;69(3):929–940.
[11] Vizitiu IC. Sidelobe reduction in the pulse-compression radar using synthesis of NLFM laws. Int J Antennas Propag. 2013;2013:1–9. DOI:10.1155/2013/605604
[12] Cook CE, Paolillo J. A pulse compression predistortion function for efficient sidelobe reduction in a high-power radar. Proceedings of the IEEE. 1964;52(4):377–389.
[13] Collins T, Atkins P. Nonlinear frequency modulation chirps for active sonar. IEE Proceedings – Radar, Sonar and Navigation. 1999;146(6):312–316.
[14] Ghavamirad R, Sebt MA. Sidelobe level reduction in acf of nlfm waveform. IET Radar, Sonar Navigation. 2019;13(1):74–80.
[15] Beauchamp RM, Tanelli S, Peral E, et al. Pulse compression waveform and filter optimization for spaceborne cloud and precipitation radar. IEEE Trans Geosci Remote Sens. 2017;55(2):915–931.
[16] Blunt SD, Mokole EL. Overview of radar waveform diversity. IEEE Aerospace Electron Syst Magazine. 2016;31(11):2–42.
[17] Ghavamirad R, Sebt MA, Babashah H. Phase improvement algorithm for nlfm waveform design to reduction of sidelobe level in autocorrelation function. Electron Lett. 2018;54(18):1091–1093.
[18] Huang D, Leung H, Huang X. Experimental evaluation of predistortion techniques for high-power amplifier. IEEE Trans Instrum Meas. 2006;55(6):2155–2164.
[19] Netterstrom A. Using digital pre-distortion to compensate for analog signal processing errors. IEEE International Conference on Radar; 1990. p. 243–248
[20] Dunn Z, Yeary M, Fulton C, et al. Wideband digital predistortion of solid-state radar amplifiers. IEEE Trans Aerosp Electron Syst. 2016;52(5):2452–2466.
[21] Scheiblhofer S, Schuster S, Stelzer A. High-speed fmcw radar frequency synthesizer with dds based linearization. IEEE Microw Wirel Compon Lett. 2007;17(5):397–399.
[22] Kim J, Konstantinou K. Digital predistortion of wideband signals based on power amplifier model with memory. Electron Lett. 2001;37(23):1417–1418.
[23] Morgan DR, Ma Z, Kim J, et al. A generalized memory polynomial model for digital predistortion of rf power amplifiers. IEEE Trans Signal Process. 2006;54(10):3852–3860.
[24] Gumber K, Rawat M. Low-cost rfin-rfout predistorter linearizer for high-power amplifiers and ultra-wideband signals. IEEE Trans Instrum Meas. 2018;67(9):2069–2081.
[25] Rawat M, Rawat K, Ghannouchi FM, et al. Generalized rational functions for reduced-complexity behavioral modeling and digital predistortion of broadband wireless transmitters. IEEE Trans Instrum Meas. 2014;63(2):485–498.

[26] Doerry AW. Generating precision nonlinear FM chirp waveforms. In: Kurtz JL, Tan RJ, editors. Radar Sensor Technology XI; Apr. SPIE; 2007. DOI:10.1117/12.717796
[27] Jackson L, Kay S, Vankayalapati N. Iterative method for nonlinear fm synthesis of radar signals. IEEE Trans Aerosp Electron Syst. 2010;46(2):910–917.
[28] Eaves JL, Reedy EK. Principles of modern radar. US: Springer; 1987. DOI:10.1007/978-1-4613-1971-9
[29] Singh AK, Kim YH. Methods of wideband chirp signal generation using fpga. International Conference on Computing, Communication Automation; 2015. p. 1243–1247
[30] Sun B, Yeary M, Uysal F, et al. Digital radar implementation with amplitude predistortion. 2017 IEEE Radar Conference (RadarConf); 2017. p. 1691–1696